

---

# Arbitrary Lagrangian-Eulerian (ALE) Method in Cylindrical Coordinates for Laser Plasma Simulations

Milan Kucharik<sup>1</sup>, Richard Liska<sup>2</sup>, Raphael Loubere<sup>3</sup>, and Mikhail Shashkov<sup>1</sup>

<sup>1</sup> Los Alamos National Laboratory, Los Alamos, NM 87545, USA  
kucharik@lanl.gov, shashkov@lanl.gov

<sup>2</sup> Czech Technical University, Faculty of Nuclear Sciences and Physical  
Engineering, Břehová 7, 115 19 Prague 1, Czech Republic  
liska@siduri.fjfi.cvut.cz

<sup>3</sup> Universite Paul-Sabatier Toulouse 3, Maths pour l'Industrie et la Physique MIP,  
31062 Toulouse Cedex 9, France loubere@mip.ups-tlse.fr

**Summary.** The Cartesian arbitrary Lagrangian-Eulerian (ALE) method is generalized to cylindrical coordinates and implemented on logically rectangular quadrilateral mesh. For laser plasma applications the code is extended to model also laser absorption and heat conductivity. The code is used for simulation of high velocity impact problem for which pure Lagrangian method fails due to severe mesh distortion.

## 1 Introduction

For solving of compressible fluid equations, one can use two different approaches – the Eulerian and Lagrangian methods. In the Eulerian approach, the fluid flows through a static computational mesh, in the Lagrangian approach, the computational mesh moves with the fluid, there is no mass flux between computational cells. The advantage of the Lagrangian approach is obvious – it can simulate situations when the investigated fluid considerably changes its volume (like compression or expansion) or its shape and when moving boundary conditions are treated naturally. This is exactly the situation in laser-plasma simulations, where the computational domain dramatically changes during target compression or corona expansion, and thus the Lagrangian approach is convenient. Unfortunately, the moving computational mesh can degenerate or even tangle during the simulation, it can lose its regularity, and the Lagrangian computation cannot continue as its assumptions on the mesh quality do not remain valid.

The Arbitrary Lagrangian-Eulerian (ALE) [1] method combines positives of both approaches to treat this problem. The computational mesh moves as in

the Lagrangian approach, so one can treat changing computational domains. When mesh quality decreases, the Eulerian part of the ALE method comes into play – the mesh is rezoned (smoothed), and the conservative quantities are conservatively remapped to a new, smoothed mesh. Then, the Lagrangian step can continue till the next mesh smoothing step.

In [2], we presented the ALE method in Cartesian geometry, working on quadrilateral 2D computational meshes. Here we extend this ALE method to the cylindrical  $r-z$  geometry needed for modeling of laser plasma interactions. The laser plasma is modeled by the Lagrangian hydrodynamical equations

$$\begin{aligned} \frac{d\rho}{dt} + \rho \operatorname{div} \mathbf{u} &= 0, & \rho \frac{d\mathbf{u}}{dt} + \mathbf{grad} p &= 0 \\ \rho \frac{d\epsilon}{dt} + p \operatorname{div} \mathbf{u} &= -\operatorname{div}(\mathbf{I}) + \operatorname{div}(\kappa \mathbf{grad} T) \end{aligned} \quad (1)$$

where  $\rho$  is density,  $\mathbf{u}$  velocity,  $p$  pressure,  $\epsilon$  specific internal energy,  $T$  temperature,  $\kappa$  heat conductivity and  $\mathbf{I}$  vector of laser intensity. The total Lagrangian time derivatives in this system include convective terms  $d/dt = \partial/\partial t + \mathbf{u} \cdot \mathbf{grad}$ . The movement of each node of the Lagrangian mesh is defined by an ordinary differential equation  $d\mathbf{x}(t)/dt = \mathbf{u}$ . The system is closed by the equation of state defining relations  $p = p(\epsilon, \rho), T = T(\epsilon, \rho)$  between thermodynamical quantities  $\epsilon, \rho, p, T$ . This system is numerically treated by splitting it into hyperbolic and parabolic (heat conductivity) parts.

## 2 Lagrangian Step

Lagrangian hyperbolic hydrodynamical equations are numerically treated by a compatible staggered method [3] which defines the scalar quantities ( $\rho, p, \epsilon, T$ ) inside grid cells, and the vector quantities ( $\mathbf{x}, \mathbf{u}$ ) in grid nodes. There are two versions of the compatible method in the cylindrical  $r-z$  geometry [3]: Area Weighted (AW) and Control Volume (CV) methods. The AW method cannot be used in the ALE framework as it does not define well the cylindrical volumes needed during remapping and without these volumes we are not able to construct an AW compatible remapping.

The CV method defines the quadrilateral cell volume (based on Green's theorem)

$$V_c = \int_c 1 r dr dz = \frac{1}{6} \sum_{l=1}^4 (z_{l+1} - z_l) (r_l^2 + r_{l+1}^2 + r_l r_{l+1}) \quad (2)$$

where  $(r_l, z_l), l = 1, \dots, 4$  (with cyclic extension) are the coordinates of four nodes defining the cell  $c$ . However, the cylindrical CV method has to be modified to be compatible with ALE remapping. Originally the CV method defines cell center as the average of the cell nodes. The average is replaced by the mass center of the cell

$$r_c = \frac{1}{V_c} \int_c r^2 dr dz, \quad z_c = \frac{1}{V_c} \int_c z r dr dz$$

so that the remapping can be conservative. The compatible method is based on the zonal, subzonal, and viscosity forces in each grid node. The cell integrals appearing in the zonal and subzonal forces in cylindrical geometry contain additional factor  $r$  compared to the Cartesian geometry case. Using Green's theorem the cell integrals are transformed into the integrals over the cell edges which are evaluated exactly (see below).

### 3 Rezoning and Remapping

The rezoning stage of the ALE method performs mesh smoothing. Most often we employ the simple Winslow smoothing technique [4] for rezoning, like in Cartesian geometry, even though more advanced methods as the reference Jacobian approach exist. Special boundary conditions in cylindrical geometry are applied during rezoning on the  $z$  axis so that the boundary nodes movement is constrained to this axis.

The remapping stage of the ALE method includes a conservative interpolation of the discrete conserved quantities from an old mesh to a new smoother one. The remapping stage consists of three steps: reconstruction, integration and repair. First the remapped conservative function  $g$  (as e.g. density  $\rho$ ) is reconstructed from the discrete values by a piecewise linear function on each old cell, typically with the Barth-Jespersen limiter. Then the reconstructed piecewise linear function is integrated over each new cell  $\tilde{c}$  (objects related to the new mesh are accented by a tilde) to get the total value  $G_{\tilde{c}} = \int_{\tilde{c}} g r dr dz$  of the conserved quantity (e.g. mass of the cell) inside the new cell, which defines the remapped density of conserved quantity  $\tilde{g}_{\tilde{c}} = G_{\tilde{c}}/V_{\tilde{c}}$ .

The natural exact integration of the piecewise linear function over the new cell requires computing intersections of the new cell with all neighboring old cells, see Fig. 1(a) where the new cell  $\tilde{c}_{i,j} = \tilde{P}_{i,j}, \tilde{P}_{i+1,j}, \tilde{P}_{i+1,j+1}, \tilde{P}_{i,j+1}$  intersects with nine ( $3 \times 3$  patch) old cells  $c_{k,l}, k = i-1, i, i+1, l = j-1, j, j+1$ . The linear reconstruction, given by the old cell  $c'$

$$g(r, z) = g_{c'} + \left( \frac{\partial g}{\partial r} \right)_{c'} (r - r_{c'}) + \left( \frac{\partial g}{\partial z} \right)_{c'} (z - z_{c'}),$$

inside each such intersection  $I_{c'}^{\tilde{c}}$  results in the contribution

$$\begin{aligned} G_{I_{c'}^{\tilde{c}}} = & g_{c'} \int_{I_{c'}^{\tilde{c}}} r dr dz + \left( \frac{\partial g}{\partial r} \right)_{c'} \left( \int_{I_{c'}^{\tilde{c}}} r^2 dr dz - r_{c'} \int_{I_{c'}^{\tilde{c}}} r dr dz \right) \\ & + \left( \frac{\partial g}{\partial z} \right)_{c'} \left( \int_{I_{c'}^{\tilde{c}}} z r dr dz - z_{c'} \int_{I_{c'}^{\tilde{c}}} r dr dz \right) \end{aligned} \quad (3)$$

to the whole integral  $G_{\tilde{z}}$ . The integrals in this contribution over the polygonal intersection are transformed using Green's theorem into integrals over the edges of the polygon. The exact integration is computationally rather expensive because it requires finding all cell intersections.

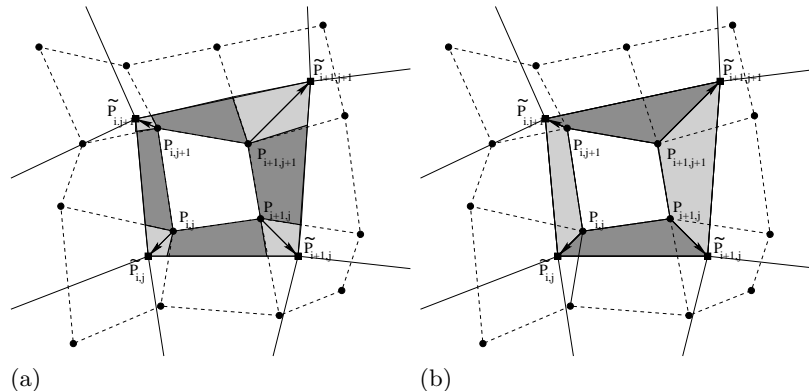


**Fig. 1.** Old (dashed) and new (solid segments) mesh with intersection regions for the exact integration (a) and swept regions for the approximate integration (b).

The approximate integration over swept regions (see [5] for Cartesian geometry case), which are the regions swept by the cell edges moving from old mesh to the new position in the new mesh (see Fig. 1(b)), is much faster. The contribution from each of the four swept regions has similar form as (3) with the intersection  $I_{\tilde{c}}$  replaced by the swept region. Green's theorem again transforms integrals over polygons into integrals over the edges of the polygon. In all the cases the integration from the Lagrangian step and from the remapping, the integrals of low degree polynomials in  $r, z$  over the given polygon  $P$  can be exactly evaluated as e.g. (2) or

$$\int_P r^2 dr dz = \frac{1}{12} \sum_{e \in \partial P} (z_2 - z_1) (r_1^2 + r_2^2) (r_1 + r_2)$$

$$\int_P z r dr dz = \frac{1}{24} \sum_{e \in \partial P} (z_2 - z_1) (r_1^2 (3z_1 + z_2) + r_2^2 (3z_2 + z_1) + 2r_1 r_2 (z_1 + z_2)),$$

where the edge  $e$  connects the polygon  $P$  vertexes  $(r_1, z_1)$  and  $(r_2, z_2)$ . In the swept regions method the integrals of the reconstructed function over the swept regions can be interpreted as fluxes through the mesh edges and the remapping formula can be written in a conservative flux form.

The last step of the remapping phase is repair [6] which conservatively redistributes conserved quantities in such a way that the remapping does not introduce any new local extrema.

## 4 Laser Absorption and Heat Conductivity

For laser plasma simulations, several more issues have to be included to get realistic results. The first is the model of laser absorption which appears as a source term  $\text{div}(\mathbf{I})$  in the energy equation (1). We assume that the absorption appears only on a critical surface which is the isosurface with a critical density. The laser penetrates through the subcritical density where its intensity is given by laser radial and temporal profiles. Behind the critical surface the laser intensity is zero. The laser intensity is projected on the edge normals at the edge midpoints and  $\text{div}(\mathbf{I})$  approximated by the standard formula (derived from Green's theorem) is included as a source in the hyperbolic part of the energy equation (1) in Lagrangian step.

The simulation of laser absorption is considerably influenced by plasma heat conductivity which is included as a parabolic term in the energy equation (1). The parabolic part of the energy equation is treated separately by splitting by an implicit mimetic finite difference method [7] generalized to cylindrical geometry. The mimetic method works well on poor quality meshes appearing quite often in the Lagrangian simulations and it can resolve the heat waves caused by non-linear heat conductivity  $\kappa(T)$ , which is typically proportional to  $T^{5/2}$  for plasma.

## 5 Simulations of flyer targets

To show the ability of our cylindrical code to perform complex modeling of the laser-plasma interactions, we simulated a set of problems based on the real experiments [8] performed at the PALS laser facility in Prague. Here we shortly present one of these simulations. A thin Aluminum disc is irradiated by an intense laser beam and ablatively accelerated up to a very high speed. The disc flyer impacts the massive Aluminum target creating a crater. The experimental setup is shown in Fig. 2(a). The Aluminum disc flyer has radius  $r = 150 \mu\text{m}$  and thickness  $d = 11 \mu\text{m}$  and is originally placed at distance  $L = 200 \mu\text{m}$  from the massive Aluminum target. The laser operates at 3-rd harmonics with a total energy 240 J, the laser pulse length is 400 ps and radius of focus (laser spot on target) is  $r_f = 125 \mu\text{m}$ .

We split the simulation into two parts. In the first part the disc flyer is ablatively accelerated by the laser beam and in the second part the impact of the disc flyer into the massive target is modeled. The laser absorption heats the upper disc surface which evaporates and expands upwards very rapidly, accelerating the disc downwards due to momentum conservation. The first part of the simulation is stopped at time  $t = 1.3 \text{ ns}$  when the disc reaches the massive target as shown in Fig. 2(b) and zoomed at Fig. 3(a). The average velocity of the disc flyer impacting the target is 134 km/s. Note in Fig. 2(b) that the size of the computing domain has expanded from  $d = 11 \mu\text{m}$  to  $2000 \mu\text{m}$  in  $z$  direction and from  $r = 150 \mu\text{m}$  to more than  $1500 \mu\text{m}$  in  $r$

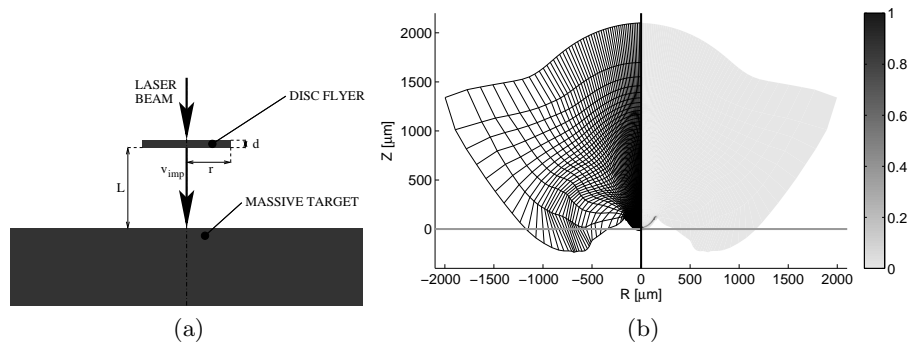


**Fig. 2.** Experimental setup (a); mesh and density colormap of the accelerated disc flyer hitting the massive target (b) where the horizontal line at  $z = 0$  marks the upper surface of the target.

direction showing the need to use the Lagrangian moving mesh formulation. Similar expansion rate appears also during the second part of simulation, the huge area of reflected material moving upwards is cut off in Fig. 4 in order to be able to distinguish the features of the crater.

The initial conditions for the impact simulation, shown in Fig. 3(b), are obtained by a conservative interpolation from the results of the ablative disc acceleration, shown in Fig. 3(a), to the initial mesh constructed for impact simulation. The impact simulation by pure Lagrangian method fails soon after time 0.5 ns due to a seriously distorted computational mesh, shown in Fig. 3(c), while the ALE method keeps the mesh reasonably smooth as seen in Fig. 3(d). The impact simulation is possible only by the ALE method. After the impact the large kinetic energy of the disc flyer is transformed into an internal energy which melts and evaporates the target material. The circular shock wave visible in the solid phase region in Fig. 4 propagates into the massive target. The computational mesh and temperature colormap is presented in Fig. 4 at time  $t = 80$  ns. The temperature colormap is separated by two temperature isolines, corresponding to Aluminum melting and evaporating temperature, into three regions (from bottom to top on  $z$  axis) of solid, liquid and gas phases. The crater is formed by the impact in the target. We interpret the crater boundary by the gas - liquid interface. After time  $t = 80$  ns this interface does not move any further into the target, so that the upper temperature isoline in Fig. 4 presents the final shape of the simulated crater. The simulated crater formations are reasonably similar to the experimental data. More physics related details can be found in [9, 10].

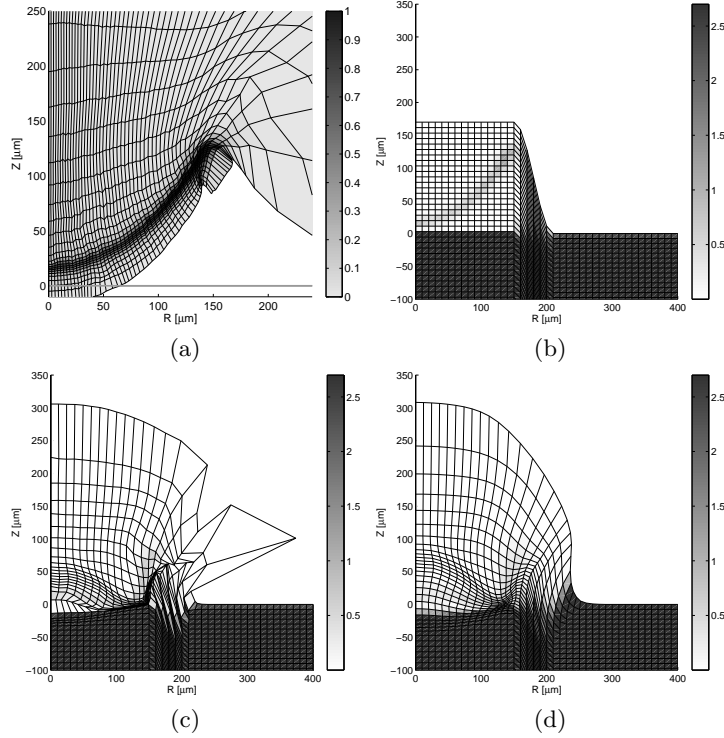


**Fig. 3.** Density colormaps of: the accelerated disc flyer hitting the massive target (a) (zoomed Fig. 2(b)); the initial conditions and the mesh for the impact simulation (b); impact simulation at  $t = 0.5$  ns by pure Lagrangian (c) and ALE method (d).

## 6 Conclusion

All parts of the ALE method have been generalized from Cartesian to cylindrical geometry and implemented into the 2D laser plasma simulation code including also heat conductivity and laser absorption. The code has been applied to the simulations of the disc flyer targets originated from PALS experiments. The pure Lagrangian method without ALE extension is unable to simulate such high velocity impact problems due to severe mesh distortion appearing very soon after the impact, while ALE gives results which compare reasonably well with the experimental data.

**Acknowledgment:** This work was carried out under the auspices of the National Nuclear Security Administration of the U.S. Department of Energy at Los Alamos National Laboratory under Contract No. DE-AC52-06NA25396. This research has been partly supported by the Czech Ministry of Education project MSM 6840770022, research center LC 528 and the Czech Science Foundation project GACR 202/03/H162.

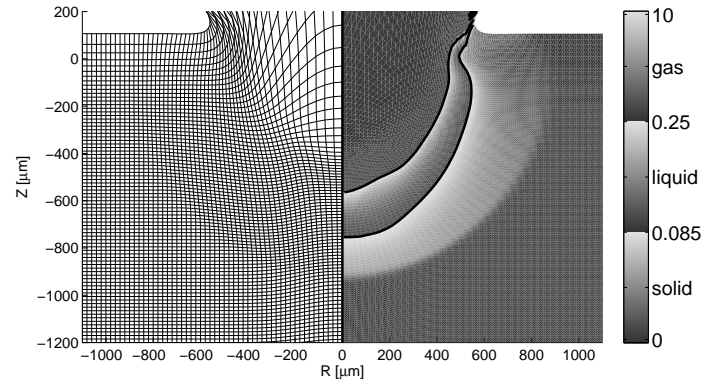


**Fig. 4.** Computational mesh (only every second edge in each logical direction is visible) and temperature (in eV) colormap at time  $t = 80$  ns after the impact. Solid, liquid and gas phases (ordered on the  $z$  axis at  $R = 0$  from bottom to top) are separated by isolines at temperature of melting and evaporation of Aluminum.

## References

1. C. W. Hirt, A. A. Amsden, and J. L. Cook. An arbitrary Lagrangian-Eulerian computing method for all flow speeds. *J. Comp. Phys.*, 14:227–253, 1974. Reprinted at *J. Comp. Phys.*, 135:203–216, 1997.
2. M. Kuchařík, R. Liska, and M. Shashkov. Conservative remapping and ALE methods for plasma physics. In F. Asakura, H. Aiso, S. Kawashima, A. Matsumura, S. Nishibata, and K. Nishihara, editors, *Hyperbolic Problems: Theory, Numerics and Applications II*, pages 133–140. Osaka University, Yokohama Publishers, 2006.
3. E. J. Caramana, D. E. Burton, M. J. Shashkov, and P. P. Whalen. The construction of compatible hydrodynamics algorithms utilizing conservation of total energy. *J. Comp. Phys.*, 146(1):227–262, 1998.
4. A. M. Winslow. Equipotential zoning of two-dimensional meshes. Technical Report UCRL-7312, Lawrence Livermore National Laboratory, 1963.
5. M. Kuchařík, M. Shashkov, and B. Wendroff. An efficient linearity-and-bound-preserving remapping method. *J. Comp. Phys.*, 188(2):462–471, 2003.
6. Mikhail Shashkov and Burton Wendroff. The repair paradigm and application to conservation laws. *J. Comp. Phys.*, 198(1):265–277, 2004.
7. M. Shashkov and S. Steinberg. Solving diffusion equation with rough coefficients in rough grids. *J. Comp. Phys.*, 129:383–405, 1996.
8. S. Yu. Guskov and et.al. Investigation of shock wave loading and crater creation by means of single and double targets in PALS-laser experiment. *J. of Russian Laser Research*, 26:228–244, 2005.
9. M. Kuchařík, J. Limpouch, and R. Liska. Cylindrical 2D ALE simulations of laser interactions with flyer targets. *Czech. J. Phys.*, 56:B522–B527, 2006.
10. M. Kuchařík, J. Limpouch, and R. Liska. Laser plasma simulations by arbitrary Lagrangian Eulerian method. *J. de Physique IV*, 133:167–169, 2006.